Direct Fabrication of Large Micropatterned Single Crystals

Joanna Aizenberg,[1]* David A. Muller,[1] John L. Grazul,[1] D. R. Hamann[1,2]

Micropatterning of single crystals for technological applications is a complex, multistep process. Nature provides alternative fabrication strategies, when crystals with exquisite micro-ornamentation directly develop within preorganized frameworks. We report a bio-inspired approach to growing large micropatterned single crystals. Micropatterned templates organically modified to induce the formation of metastable amorphous calcium carbonate were imprinted with calcite nucleation sites. The template-directed deposition and crystallization of the amorphous phase resulted in the fabrication of millimeter-sized single calcite crystals with sub–10-μm patterns and controlled crystallographic orientation. We suggest that in addition to regulating the shape, micropatterned frameworks act as sites for stress and impurity release during the amorphous-to-crystalline transition. The proposed mechanisms may have direct biological relevance and broad implications in materials synthesis.

Single crystals patterned at the micrometer and nanoscale are important components in various electronic, sensory, and optical devices. The current technological fabrication strategy for these structures, so-called top-down manufacturing, is a multistep process involving the growth of a bulk single crystal and its cutting and polishing in preferred crystallographic orientations, followed by patterning procedures that include the "writing" of desired patterns on the surface by lithographic techniques and their engraving into the crystal using various etching procedures (*1*, *2*). Of the many challenges facing crystal science, the development of alternative, bottom-up crystallization strategies that would enable the direct growth of crystals with pattern remains an attractive, but elusive, goal.

In contrast to the technological world, biological systems provide numerous examples of micropatterned inorganic materials that directly develop into their intricate architectures (*3*, *4*). This ability is illustrated by skeleton formation in echinoderms (*3*–*5*): Each skeletal structural unit (spines, test plates) is composed of a single calcite crystal delicately patterned on the micrometer scale (Fig. 1). The crystallographic orientation of these crystals is under strict biological control and often has direct functional significance. For example, sophisticated arrays of microlenses formed by brittlestars (Fig. 1) are oriented along the optical *c* axis of the constituent birefringent calcite crystal. Such orientation prevents double-image formation and, therefore, improves the optical performance of the lenses (*6*).

On the basis of current knowledge of the processes that regulate crystal formation in biological environments, we can identify three general biomineralization principles. (i) Biocrystals usually grow inside organic frameworks that confine mineral deposition within predetermined spatial patterns (*3*). (ii) In certain systems, the formation of single calcite crystals takes place through the transformation of a transient amorphous calcium carbonate (ACC) phase (*7*–*9*). (iii) Control of crystallographic orientation is achieved through oriented nucleation at well-defined, chemically modified intracellular sites (*4*, *7*). A key tenet of biomineralization that unites all these processes is that the crystal formation is controlled at the molecular level by organized assemblies of specialized, organic molecules (*3*). Borrowing from these three biomineralization principles, we have developed a crystallization strategy that relies upon the design of a micropatterned, chemically modified framework that serves several functions: It induces the formation of a metastable ACC film with the predetermined micropattern, defines the location and crystallographic orientation of the calcite nucleus, relaxes the tensile stress in the deposited film, and provides discharge sites for excess water and other impurities during the crystallization process. This strategy allowed us to directly fabricate large (~1 mm), single crystals of calcite with sub–10-μm patterns and controlled crystallographic orientations.

In our approach to the fabrication of micropatterned single crystals, we take advantage of a transient amorphous phase that can be deposited within an arbitrarily patterned reaction volume and thus molded into a desired shape. ACC is a metastable phase that rapidly transforms into crystalline polymorphs—calcite, vaterite, or aragonite—when formed in vitro from highly saturated solutions (*10*–*12*). In biological environments, ACC is stabilized by specialized macromolecules rich in hydroxyamino acids, glycine, glutamate, phosphate, and polysaccharides (*13*). It is either used for structural purposes in the amorphous form or transformed into calcite (*7*, *8*) and aragonite (*9*) by means of regiospecific, oriented nucleation. The amorphous-to-crystalline transition in organisms may thus be regarded as "crystallization with form and orientation," because the crystalline phase preserves the shape of the predeposited ACC and has controlled crystallographic orientation.

Recent studies have demonstrated the great potential of biological approaches in materials synthesis (*14*–*21*). The stabilization of the unstable ACC phase in vitro has been demonstrated by the addition of hydroxy- and phosphate-containing molecules, magnesium, polypeptides, or macromolecules from biogenic ACC phases to the crystallizing solution (*11*, *13*, *22*–*25*). We have also shown that the use of self-assembled monolayers (SAMs) of ω-terminated alkanethiols supported on gold or silver (*26*), as crystallization templates, results in a highly controlled, oriented nucleation of calcite in various crystallographic orientations (*27*, *28*). We therefore envisioned that $CaCO_3$ precipitation within a micropatterned framework, which had been functionalized with phosphate and hydroxyl groups to induce the formation of ACC and imprinted with a SAM nanoregion to trigger the oriented nucleation of calcite and the amorphous-to-crystalline transition, could lead to the fabrication of an oriented, micropatterned, single calcite crystal.

The fabrication procedure of a framework engineered at the nano-, micro- and macroscale is detailed in Fig. 2A. The resulting templates had a characteristic quasi-two-

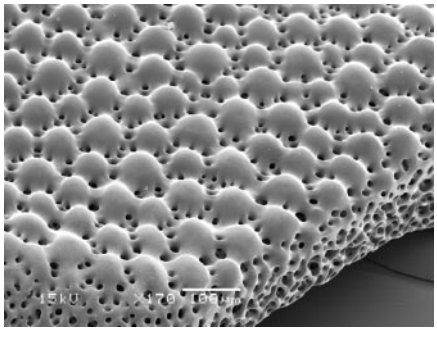

Fig. 1. Scanning electron micrograph (SEM) of a part of the skeleton of a brittlestar *Ophiocoma wendtii* (Ophioroidea, Echinodermata). The entire structure (the mesh and the array of microlenses) is composed of a single calcite crystal used by the organism for mechanical and optical functions (*6*).

[1]Bell Laboratories/Lucent Technologies, Murray Hill, NJ 07974, USA. [2]Mat-Sim Research, Murray Hill, NJ 07974, USA.

*To whom correspondence should be addressed. E-mail: jaizenberg@lucent.com

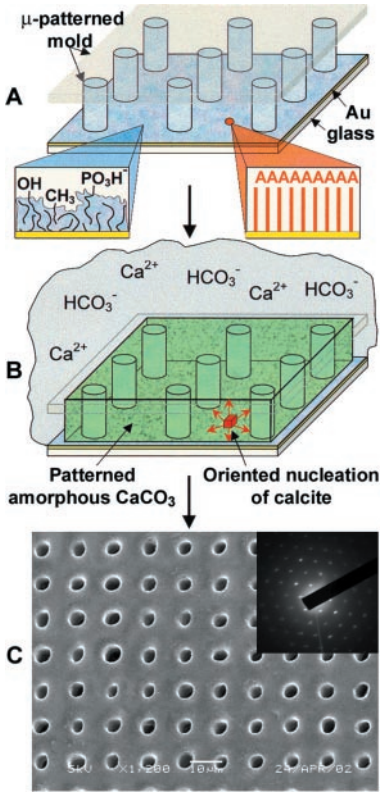

Fig. 2. Experimental setup. (**A**) Preparation of templates with q2D micropatterns for mineral deposition. Photoresist micropatterns were formed on a glass slide by standard photolithographic procedures. The micropatterns consisted of isolated photoresist features—for example, a square array of posts, with the feature sizes of <10 μm and an aspect ratio of >1. The micropatterned substrate was coated with a transparent, 5- to 10-nm-thick film of gold or silver. A nanoregion (red circle) of a SAM of $HS(CH_2)_nA$ (A = OH, CO_2H, SO_3H) that induces the nucleation of calcite in a controlled orientation (*27, 28*) was deposited on Au (Ag) by the tip of an atomic force microscope. The remainder of the surface was derivatized with a mixture of alkanethiols of different lengths terminated in phosphate, methyl, and hydroxyl groups to create a disordered organic surface that suppresses the nucleation of calcite and favors the formation of ACC. The functionalized substrate was covered with a thin, gas-permeable polymeric film, such as polydimethylsiloxane (PDMS). (**B**) Calcium carbonate deposition. The q2D substrate was placed in a 1 M $CaCl_2$ solution (pH = 7 to 9) in a closed desiccator containing $(NH_4)_2CO_3$ powder (*4, 28*). The diffusion of CO_2 through the PDMS film results in the formation of a mesh of metastable ACC in the interstices of the framework. At the preformed SAM nanoregion, calcite crystal nucleates and triggers the transformation of the ACC film. (**C**) SEM of a sample micropatterned single calcite crystal fabricated as described in (A) and (B). In the experiment shown, the photoresist pattern was a square array of 3-μm posts separated by 8-μm spaces, and the nucleation site was a SAM of $HS(CH_2)_{11}SO_3H$ on Au. The size of the holes increased from 3 μm in the amorphous film to 4.2 ± 0.5 μm in the crystal. (Inset) Large-area (~50 μm^2) TEM diffraction (*29*), showing that the section is a single crystal oriented along the *c* axis.

dimensional (q2D) geometry, which delineated interconnected reaction microchannels for subsequent inorganic crystallization (Fig. 2B). Calcium carbonate deposition was monitored in real time by optical microscopy carried out under nonpolarized light (NL) and polarized light (PL) (*29*).

Within the first 15 to 30 min, a mesh of metastable ACC filled the interstices of the framework (Fig. 3A). The amorphous character of the deposited film was inferred from its homogeneous dark appearance in PL (Fig. 3B), and it was confirmed by infrared (IR) analysis that showed broad ν_2 and ν_1 absorption bands of ACC at 865 and 1080 cm^{-1} (Fig. 4A) and by transmission electron microscopy (TEM) (*29*). In several experiments, we also added macromolecules extracted from biologically formed ACC-containing tissues (*13*), magnesium, or phosphates to stabilize the deposited ACC layer further.

Within the next 30 min, site-specific nucleation of a nascent calcite crystal occurred at the imprinted SAM nanoregion (Fig. 3B) and triggered the transformation of the ACC film. The calcite nucleus grew along the spatially delineated conduits through the ACC mesh and formed a large (up to 1 mm) micropatterned single crystal (Fig. 3C). The pore sizes in the crystal were consistently larger than the corresponding features in the original ACC film (Fig. 2C). Its single crystalline character was confirmed by large-area transmission electron diffraction data (Fig. 2C, inset). Dark-field images in diffracted beams revealed that the entire structure diffracted uniformly; i.e., no amorphous or small polycrystalline inclusions were detected (*29*). The single crystalline character is also evident from the PL movies (*29*) showing that the entire structure switches on and off simultaneously when rotated under crossed polarizers (Fig. 3D). The final size

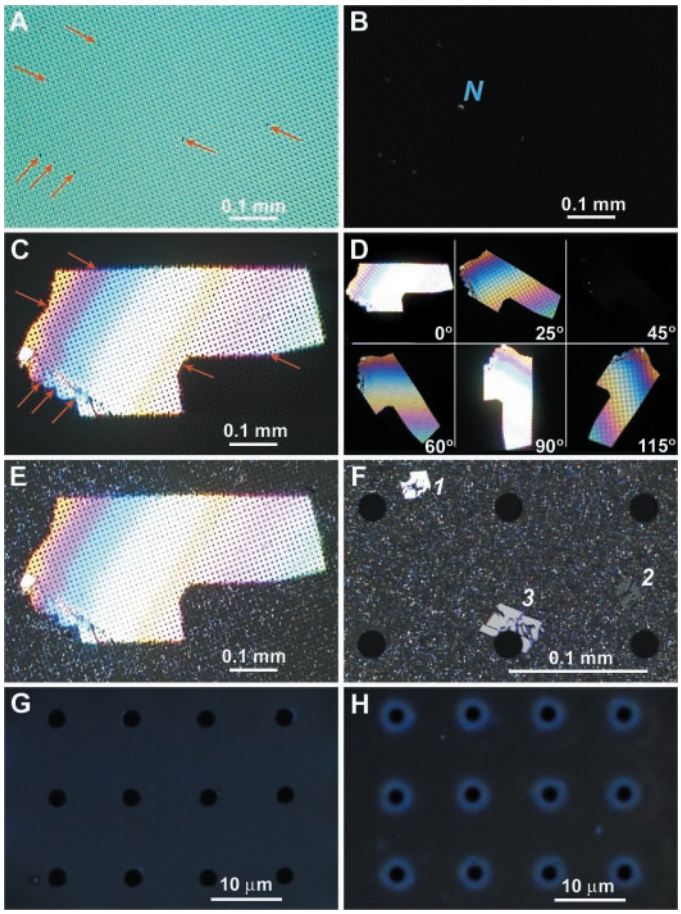

Fig. 3. Light microscopy study of the crystallization process. In the experiment shown, the photoresist pattern was a square array of 3-μm posts separated by 8-μm spaces, and the nucleation site was a SAM of $HS(CH_2)_{11}OH$ on Au. Micrographs are recorded in transmission mode. (**A** and **B**) Original, as-deposited, $CaCO_3$ layer in NL (A) and PL (B). Impurities in the film are indicated by red arrows. The homogeneous dark appearance of the mineral in PL reflects its amorphous character. The nucleus **N** is marked. (**C**) PL micrograph of the same region after 2.5 hours. Micropatterned single calcite crystal in the [104] orientation forms within the ACC film. The crystal is pinned at the impurities. (**D**) The same structure rotated under crossed polarizers. (**E**) PL micrograph of the same region after the rupture of the remaining ACC layer into a polycrystalline calcitic film. (**F**) PL micrograph of the crystallized amorphous layer in a control experiment in which a framework with large feature sizes (>15 μm) was used. In the experiment shown, three nucleation sites (**1** to **3**) were imprinted on a q2D template that consisted of an array of 20-μm posts with a periodicity of 100 μm. The formation of crystals of a characteristic size R_c = 15 to 25 μm is observed. (**G** and **H**) Fluorescence micrographs of the ACC film (G) and its corresponding calcite crystal (H) grown in the presence of a fluorescent additive in the crystallizing solution. The same integration time was used for the recording of both images. The phosphate-containing dye, 4-methylumbelliferyl phosphate, was used to ensure that the additive facilitates the ACC formation and does not create random nucleation sites (*23*). The even distribution of the dye in the ACC phase and its exclusion from the growing crystal and buildup at the posts interfaces hint at the "microsump" function of the micropatterned framework.

and macroshape of the micropatterned crystal are conceivably determined by impurities in the amorphous film that pin the crystallization front (*30*) [see arrows in Fig. 3, A and C, and crystal growth movie in (*29*)].

The crystallographic orientation is controlled at the nucleation stage by the SAM, in agreement with recent studies (*27*, *28*). X-ray diffraction measurements of the produced crystals showed the selective nucleation from the (104), (001), (015), (103), and (012) crystallographic planes by using SAMs of $HS(CH_2)_{11}OH$, $HS(CH_2)_{11}SO_3H$, or $HS(CH_2)_{15}CO_2H$ supported on Au, and SAMs of $HS(CH_2)_{11}OH$ and $HS(CH_2)_{15}CO_2H$ supported on Ag, respectively (*27*, *28*). After ~3 to 4 hours, the remaining metastable ACC film ruptured spontaneously into a micropatterned polycrystalline layer (Fig. 3E).

The mechanism of the amorphous-to-crystalline transition was studied in a series of control crystallization experiments using templates engineered with or without a nucleation site, varied feature sizes, and in the presence of additives in the solution. In the absence of the imprinted nucleation site, the ACC phase always transformed into a polycrystalline structure composed of a mixture of calcite and vaterite. The induction time for crystallization increased with the decrease of feature sizes in the micropatterned template: It was about 1 hour for nonpatterned substrates (infinite feature sizes) and increased to 4 to 5 hours when the channel diameters in the q2D template were reduced to 1 μm. The observed increase in the induction time suggests that the presence of the micropattern contributes to the stabilization of the metastable amorphous phase, most likely by providing tensile stress relaxation.

When the SAM nucleation sites were integrated into nonpatterned templates or into q2D templates with large channel diameters, calcite nuclei formed at the SAM region did not develop into micropatterned single crystals (Fig. 3F). They grew to a characteristic size R_c = 15 to 25 μm when nucleated at the distances of >15 μm from the channel edge (crystals **1** and **2** in Fig. 3F). Larger crystals formed when the nucleation site was located at distances of <15 μm from the channel edge (crystal **3** in Fig. 3F). This characteristic length scale defines the boundary condition in our experimental design: Large micropatterned single crystals can be fabricated when channel diameters in the q2D template do not exceed d = 10 to 15 μm. IR spectra of the fabricated porous crystals showed the decrease of the water absorption bands and the increase of the intensity ratio of the ν_4 and ν_2 calcite bands, with the feature sizes in the template decreasing (Fig. 4, B to E). Control experiments performed in the presence of phosphate-containing fluorescent molecules in solution showed a homogeneous distribution of the additive in the amorphous film (Fig. 3G), followed by the removal of the dye from the growing crystal and its accumulation at the framework-mineral interfaces (Fig. 3H) (*31*). The interfacial impurity buildup was also confirmed by scanning x-ray microanalysis (EDX) (*31*). These results suggest that the presence of a micropattern plays an important role also during crystal growth. Its function may include a "microsump action" for the release of water (and possibly other impurities) during the amorphous-to-crystalline transition and/or the relaxation of stress in the forming crystal.

On the basis of the experimental data, we propose the following mechanism for our crystal design strategy. The successful fabrication of a macrocrystal with controlled crystallographic orientation and micropattern relies upon the engineering of a template with essential chemical and structural features. By using appropriate surface-patterning agents, we orchestrate the formation of a transient amorphous phase with extended lifetime and control the location and properties of the nucleation site within the amorphous film. The amorphous-to-crystalline transition initiated at the imprinted nucleation site can be semiquantitatively described as follows. We consider a growing single crystal of size R in our q2D geometry. If the amorphous phase has a water concentration k, then the amount of water displaced by the crystal is increasing as kR^2 and can only be collected at the ACC-crystal interface. The interface area grows as R, and therefore the thickness L of the interfacial layer grows in proportion to R to hold the excluded water. For a true three-dimensional (3D) geometry, the amount of water displaced by the crystal increases as kR^3; the interface area grows as R^2, and therefore L also grows in proportion to R. The same scaling argument applies to the release of other possible impurities from the ACC phase. When the thickness of the interfacial water layer and/or the concentration of impurities per surface area of the crystal exceed critical values, the crystal growth in the absence of a micropattern would terminate at a characteristic crystal size of R_c (Fig. 3F).

For micropatterned templates with channel diameters $d < R_c/2$, the features may function as microsumps, at which the propagating crystallization front leaves behind the excessive water. The total sump capacity grows as R^2 in the q2D geometry or as R^3 in the 3D geometry, and the interfacial layer can then maintain an optimum water concentration. The microsump action would result in the increase of the pore diameters in the forming crystal compared with the original ACC film, as is indeed observed in our experiments (Fig. 2C). We therefore suggest that the crystallization process occurs by mass transport between the amorphous and crystalline phases, rather than by solid-state transformation. For the fabrication of crystals of better quality, the decrease in the channel diameters would be beneficial because the inclusion of water and associated stresses may result when the crystallization front travels longer distances to reach the discharge site (Fig. 4, B to E). Ideally, this controlled amorphous-to-crystalline transition would proceed isotropically, until the spontaneous crystallization of the remaining, metastable amorphous film takes place (Fig. 3E). In practice, pinning of the crystallization front at impurities (*30*) in the amorphous film occurs and thus affects the size and the shape of the growing macrocrystal.

It is noteworthy that the channel diameters $d < 10$ μm in our synthetic, micropatterned single calcite crystals are comparable with the mesh sizes observed in biologically formed single calcite crystals (Fig. 1) (*3*–*8*). This observation, coupled with the absence of large, nonporous biogenic crystals (*3*), raises an interesting possibility that the mechanistic implications proposed in this study are directly relevant to the formation of analogous structures in the biological world. When single crystals are the biomaterial of choice and their formation occurs through an amorphous phase, the development of large, solid structures is unlikely because of mechanical stresses caused by the release of water and macromolecules. A 3D array of self-assembling biological macromolecules and/or cells serving as structural templates will provide sites for stress relaxation and impurity dis-

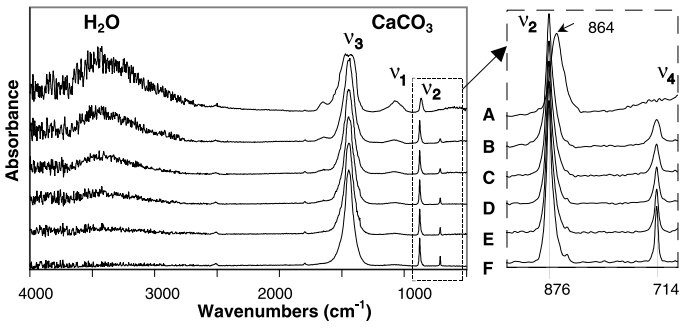

Fig. 4. Infrared spectra of $CaCO_3$ samples. The fingerprint region of $CaCO_3$ (ν_2 and ν_4 bands) is shown on the right. (**A**) Representative spectrum of the deposited ACC. (**B** to **E**) Micropatterned calcite crystals transformed from ACC with different channel diameters d: (B) 10 μm; (C) 8 μm; (D) 5 μm; (E) 2 μm. (**F**) Control spectrum of a pure, geological calcite crystal. The decrease of the water modes in patterned calcite crystals with the decrease of the feature sizes in the mold is apparent.

charge, thus giving rise to the formation of a large microporous single crystal.

In conclusion, we report here an example of direct, bottom-up synthesis of single calcite crystals with controlled orientation and microstructure. Our results suggest a general strategy for the design of micro- and nanopatterned crystalline materials: utilization of amorphous-to-crystalline transitions using specially designed structural templates with integrated nucleation sites. In our approach, the chosen micropatterned substrate not only determines the microstructure, but also is involved in the release of stresses and impurities during the formation of the final crystal. The possible applications of q2D or 3D templates may include the direct growth of defect-free micropatterned crystals, the relaxation of stresses encountered during amorphous-to-crystalline transitions in existing materials, and controlled solvent release during polycondensation reactions (*1*, *2*, *32*). Such concept transfer could perfect our ability to make nanostructured materials for a wide variety of applications and shed light on fundamental mechanisms that regulate nano- and microscale phenomena in biomineralization.

References and Notes

1. A. Gonis, Ed., *Nucleation and Growth Processes in Materials* (Materials Research Society, Boston, 2000).
2. A. W. Vere, *Crystal Growth: Principles and Progress* (Updates in Applied Physics and Electrical Technology Series, Plenum, New York, 1988).
3. H. A. Lowenstam, S. Weiner, *On Biomineralization* (Oxford Univ. Press, Oxford, 1989).
4. L. Addadi, S. Weiner, *Angew. Chem. Int. Ed. Engl.* **31**, 153 (1992).
5. F. H. Wilt, *J. Struct. Biol.* **126**, 216 (1999).
6. J. Aizenberg, A. Tkachenko, S. Weiner, L. Addadi, G. Hendler, *Nature* **412**, 819 (2001).
7. E. Beniash, J. Aizenberg, L. Addadi, S. Weiner, *Proc. R. Soc. London Ser. B* **264**, 461 (1997).
8. E. Beniash, L. Addadi, S. Weiner, *J. Struct. Biol.* **125**, 50 (1999).
9. I. M. Weiss, N. Tuross, L. Addadi, S. Weiner, *J. Exp. Zool.* **293**, 478 (2002).
10. N. Koga, Y. Z. Nakagoe, H. Tanaka, *Thermochim. Acta* **318**, 239 (1998).
11. S. Raz, S. Weiner, L. Addadi, *Adv. Mater.* **12**, 38 (2000).
12. E. Loste, F. C. Meldrum, *Chem. Commun.*, 901 (2001).
13. J. Aizenberg, G. Lambert, S. Weiner, L. Addadi, *J. Am. Chem. Soc.* **124**, 32 (2002).
14. M. Alper, P. D. Calvert, R. Frankel, P. C. Rieke, D. A. Tirrell, *Materials Synthesis Based on Biological Processes* (Materials Research Society, Pittsburgh, 1991).
15. A. H. Heuer *et al.*, *Science* **255**, 1098 (1992).
16. S. Mann *et al.*, *Science* **261**, 1286 (1993).
17. T. Douglas *et al.*, *Science* **269**, 54 (1995).
18. J. H. Fendler, *Chem. Mater.* **8**, 1616 (1996).
19. S. Mann, G. A. Ozin, *Nature* **382**, 313 (1996).
20. S. I. Stupp, P. V. Braun, *Science* **277**, 1242 (1997).
21. A. M. Belcher, P. K. Hansma, G. D. Stucky, D. E. Morse, *Acta Mater.* **46**, 733 (1998).
22. H. L. Merten, G. L. Bachman, U.S. Patent 4,237,147 (1980).
23. K. Sawada, *Pure Appl. Chem.* **69**, 921 (1997).
24. L. B. Gower, D. J. Odom, *J. Cryst. Growth* **210**, 719 (2000).
25. G. F. Xu, N. Yao, I. A. Aksay, J. T. Groves, *J. Am. Chem. Soc.* **120**, 11977 (1998).
26. A. Kumar, N. L. Abbott, E. Kim, H. A. Biebuyck, G. M. Whitesides, *Acc. Chem. Res.* **28**, 219 (1995).
27. J. Aizenberg, A. J. Black, G. M. Whitesides, *Nature* **398**, 495 (1999).
28. _____, *J. Am. Chem. Soc.* **121**, 4500 (1999).
29. Video clips and TEM data are presented as supporting online material on *Science* Online.
30. H. H. Teng, P. M. Dove, C. A. Orme, J. J. De Yoreo, *Science* **282**, 724 (1998).
31. A detailed Raman, EDX, and fluorescence microscopy study of the incorporation of impurities will be reported elsewhere.
32. T. P. L. Pedersen *et al.*, *Appl. Phys. Lett.* **79**, 3597 (2001).

33. We thank L. Addadi, S. Weiner, and G. M. Whitesides for constructive discussions.

Supporting Online Material

www.sciencemag.org/cgi/content/full/299/5610/1205/DC1
Fig. S1
Movies S1 and S2

8 October 2002; accepted 20 December 2002

Giant Supramolecular Liquid Crystal Lattice

Goran Ungar,[1]* Yongsong Liu,[1] Xiangbing Zeng,[1] Virgil Percec,[2] Wook-Dong Cho[2]

Self-organized supramolecular organic nanostructures have potential applications that include molecular electronics, photonics, and precursors for nanoporous catalysts. Accordingly, understanding how self-assembly is controlled by molecular architecture will enable the design of increasingly complex structures. We report a liquid crystal (LC) phase with a tetragonal three-dimensional unit cell containing 30 globular supramolecular dendrimers, each of which is self-assembled from 12 dendron (tree-like) molecules, for the compounds described here. The present structure is one of the most complex LC phases yet discovered. A model explaining how spatial arrangement of self-assembled dendritic aggregates depends on molecular architecture and temperature is proposed.

Molecular self-assembly into a variety of bulk phases with two-dimensional (2D) and 3D nanoscale periodicity, such as cubic, cylindrical, or mesh phases, has been researched intensely in lyotropic (e.g., surfactant-water) LCs (*1*), block copolymers (*2–4*), and thermotropic (solvent-free) LCs (*5*, *6*). Lyotropics can provide templates for porous inorganic materials with well-defined structures (*7*), and LC complexes of DNA with cationic and neutral lipids are potential carriers for gene delivery (*8*). Complex organic nanostructures (*9*, *10*) may serve as scaffolds for photonic materials (*11*) and other nanoarrays (*12*) and for surface nanopatterning (*13*). In the case of bicontinuous cubic phases (*1*, *2*, *5*), the same structures have been observed in lyotropics, thermotropics, and block copolymers. The recent inclusion of self-assembling dendrons into the category of nanostructured soft matter (*14*) has shown their tapered shape to be responsible for creating similar bulk phases (*13*, *15–18*) and enabling "self-processing" of electronics components (*19*). It has also become apparent that manipulating the size and distribution of "micelles" aggregated from self-assembling dendrons can be used in controlling polymerization (*16*). Regarding creation of structural diversity, dendron shape can be fine-tuned in ways unavailable in lyotropic LCs or block copolymers (*14*), and hence have the potential of forming hitherto unobserved phases. Here, we report a highly complex noncubic phase and develop a relationship between chemical structure and the self-assembly mode of tapered dendrons.

We concentrate on compounds **I** and **II**, labeled [4-3,4,5-(3,5)^2]12G3-X in (*20*) (Scheme 1), where X is CH_2OH and COOH, respectively. However, we have also observed the x-ray signature of the noncubic 3D phase in a number of systems, including the following dendrons: [4-3,4,5-(3,4)^2]12G3-CO_2CH_3, [4-(3,4,5)^2]12G2-COOH, (3,4-3,4,5)12G2-CH_2OH, [3,4-(3,5)^2]12G3-CH_2OH, (4-3,4,5-3,5)12G2-CH_2OH (*20*), polyoxazolines with tapered side groups containing alkyl chains of different lengths (*17*), as well as in rubidium and cesium salts of 3,4,5-*tris*-(*n*-alkoxy)benzoic acid (*21*).

Wedge-shaped dendrons such as **I** and **II**, having alkyl tails on their periphery, have so far been found to form either columnar or cubic phases. In the former, dendrons assemble like flat pizza slices into disks, which stack into columns, which in turn form a hexagonal array. Dendrons with more alkyl chains are cone-shaped and assemble into supramolecular spheres. So far, these spherical aggregates have been known to pack on two cubic lattices, one with $Pm\bar{3}n$ and the

[1]Department of Engineering Materials, University of Sheffield, Sheffield S1 3JD, UK. [2]Roy and Diana Vagelos Laboratories, Department of Chemistry, University of Pennsylvania, Philadelphia, PA 19104–6323, USA.

*To whom correspondence should be addressed. E-mail: g.ungar@shef.ac.uk